Role of magnetic anisotropy in the ultrafast magnetization dynamics of Gd-Fe thin films of different thicknesses

Sucheta Mondal,[1] Abhishek Talapatra,[2] J. Arout Chelvane,[3] Jyoti Ranjan Mohanty,[2] and Anjan Barman[1,*]

[1]*Department of Condensed Matter Physics and Material Sciences, S. N. Bose National Centre for Basic Sciences, Block JD, Sector III, Salt Lake, Kolkata 700106, India*

[2]*Nanomagnetism and Microscopy Laboratory, Department of Physics, Indian Institute of Technology Hyderabad, Kandi, Sangareddy, 502285 Telangana, India*

[3]*Defence Metallurgical Research Laboratory, Kanchanbagh, Hyderabad 500058, India*

(Received 11 June 2019; revised manuscript received 6 August 2019; published 26 August 2019)

The time-resolved magneto-optical Kerr effect technique has been exploited to study the magnetization dynamics over femtosecond to nanosecond timescale for Gd-Fe thin films with different thicknesses. The precessional magnetization dynamics is studied by varying the magnitude and orientation of the bias magnetic field from nearly in-plane to nearly out-of-plane (OOP) direction. The analysis of bias magnetic field dependence of precessional frequency has revealed the development of OOP anisotropy when the film thickness was increased from 20 to 100 nm and this is in good agreement with the static magnetic properties of the films. Moreover, the 100-nm-thick film has shown a signature of perpendicular standing spin wave modes along with the uniform Kittel mode. The evolution of their frequency, decay time, and damping with the magnitude and orientation of bias magnetic field is analyzed in detail, showing possible energy transfer between the perpendicular standing spin wave modes and the uniform Kittel mode. Interestingly, the effective damping could be tuned over a broader range of 0.02 to 0.15, which shows the potential for applications in miniaturized and fast magnetic storage, magnetic memory, and magnonic devices.

DOI: 10.1103/PhysRevB.100.054436

I. INTRODUCTION

The possibilities of manipulating a magnetic system without applying external magnetic field have gained considerable research interest during the last two decades due to their potential applications in magnetic storage devices. Some familiar examples include spin polarized current induced spin-transfer torque (STT) switching [1], electric field controlled magnetic devices [2], and all-optical switching (AOS) of magnetization in an ultrafast timescale using ultrashort laser pulses [3]. Optical control of magnetic order by femtosecond (fs) laser pulses has become an exciting and expanding research field as it explores faster ways for magnetization reversal in a subpicosecond (ps) timescale. This was not achieved from the precessional switching of the magnetization in the presence of an orthogonal external magnetic field. A realistic switching time, which can be achieved in such a process, is on the order of 100 ps and is determined by the strength and duration of the magnetic field pulse [4–6]. There are three fundamental effects of ultrafast stimuli on a magnetic system, namely, ultrafast demagnetization, AOS, and laser-induced spin precession and damping. Since the report on ultrafast demagnetization in Ni films by Beaurepaire *et al.*, the mechanism behind this has become a topic of intense debate [7]. Unlike the transient change in magnetization described by ultrafast demagnetization, Stanciu *et al.* demonstrated a complete reversal of magnetization in rare-earth (RE) and transition-metal (TM) alloys employing optical stimuli in the absence of an external magnetic field [8]. All-optical helicity dependent switching thus promises a rapid increase in writing speed for magnetic recording devices [3]. This has widely been studied in the last decade for various magnetic thin films including perpendicularly magnetized multilayers, synthetic antiferromagnets, and different ferromagnetic alloys [9,10]. The dynamics of the magnetization precession allows direct access to study the magnetic anisotropy, damping, and precessional frequency of different dynamic modes, such as the uniform Kittel mode, the perpendicular standing spin wave (PSSW) mode and other dispersive modes in a continuous thin film [11,12] and patterned nanostructures [13]. Control of Gilbert damping by various external stimuli has been demonstrated [14–19], which shows their applications in spintronic and magnonic devices. The magnetization dynamics becomes further intriguing in the case of multisublattice magnets, where an important role is played by the exchange of angular momentum between the nonequivalent sublattices after being stimulated. Alloys of $3d$ TM and $4f$ RE metals are at the center of attraction because they exhibit tunable magnetic properties with the change in stoichiometry [20–24]. This behavior with a strong magneto-optic effect makes them particularly interesting for magneto-optical recording when they exhibit perpendicular magnetic anisotropy (PMA) [25,26]. Another aspect of technological interest is higher magnetostriction with in-plane (IP) anisotropy, which makes them applicable in magnetostrictive memory [27,28], sensors, and actuators. Among such RE-TM alloy systems, it is observed that the timescale of magnetization dynamics is dependent on the

*abarman@bose.res.in

exchange interaction and the balance of angular momentum between the RE and TM sublattices, particularly when they display antiferromagnetic coupling [20]. This provides an excellent opportunity to study the element-specific response of the materials using x-ray probes [21]. Gd-Fe based ferrimagnetic alloys are potential candidates for magneto-optic media, bubble memories, and those are scientifically rich due to the antiferromagnetic coupling between the Gd and Fe sublattices. Thus, substantial effort has been made to explore the composition dependent nature of ultrafast demagnetization and remagnetization in this system aiming towards a decrease in switching time [22]. On the other hand, the role of a higher magnetic field in the study of magnetization dynamics has been explicitly observed by Becker and colleagues in the context of RE-TM alloys [29]. The role of RE concentration and pump fluence on the Gilbert damping have also been reported for these alloys [30,31]. Substantial research has been performed to study the magnetic domains [32] and spin reorientation transition with external perturbations [33,34] for amorphous Gd-Fe thin films. However, a systematic investigation of magnetization dynamics as a function of film thickness with special emphasis towards understanding of the dynamic modes and their damping behavior has not been reported, to our knowledge, for the Gd-Fe system.

This paper aims at systematic investigation of ultrafast magnetization dynamics in Gd-Fe thin films with different thicknesses viz., 20, 50, and 100 nm employing time-resolved magneto-optical Kerr effect (TRMOKE) technique with two-color pump-probe geometry. Here, we report the overall ultrafast demagnetization time and remagnetization times of Gd-Fe system. The bias magnetic field dependence of the precessional frequency of the Kittel mode for lower thickness and several standing spin-wave (SW) modes in the higher thickness regime is studied for different field orientation. The frequency dependence of damping of the Kittel mode and decay constants, for both Kittel and PSSW modes has been explicitly demonstrated. The out-of-plane (OOP) magnetic anisotropy is found to be developed in these films with increasing thickness, which influences the magnetization dynamics significantly. Importantly, the tunability of the orientations of magnetization with applied field for different thicknesses of Gd-Fe films has also been shown from the field-dispersion relations. It should be noted that all the experiments are performed at room temperature, which is below the compensation point of the considered Gd-Fe films and hence we essentially probe the net ferromagnetic moment of the system instead of considering the magnetization of the individual sublattice and the antiferromagnetic coupling between them. The mutual energy transfer mechanism between the PSSW modes and the uniform Kittel mode is reported for Gd-Fe thin films showing evolution with magnetic field strength.

II. EXPERIMENTAL METHODS

A. Sample preparation and static characterizations

Gd-Fe thin films of thicknesses $d = 20,\ 50$, and 100 nm were deposited by electron-beam (e-beam) evaporation at room temperature on Si (100) substrates with background pressure better than 2×10^{-6} Torr. The growth rate of the films was set at around 0.3 nm/s employing an alloy target of equiatomic elemental composition Gd and Fe. The substrate was rotated at a constant speed of 10 rpm in order to ensure the uniformity in thickness. A 3-nm-thin layer of Cr was deposited as a capping layer.

The e-beam evaporated Gd-Fe films are amorphous in nature [33] and the stoichiometry (using energy dispersive x-ray spectroscopy) has been recorded in Table I, which shows that the films are Fe-rich irrespective of their thickness. The root mean square roughness (R_q) of the films was measured by atomic force microscopy and found to be about 1 nm for all three films. The IP and OOP hysteresis loops for the Gd-Fe films measured from vibrating sample magnetometry (VSM) are shown in Fig. 1(a) and also in Fig. 1S of the Supplemental Material [35]. The values for the extracted magnetic properties have also been recorded in Table I. Lesser coercivity (H_C) indicates the soft magnetic characteristic of the samples, which reverses the magnetization at a low field (listed in Table I). It is worth mentioning that the lower values of H_C essentially confirm the state of saturation with uniform magnetization for the magnetic field values applied in the dynamic measurements.

The remanent magnetization (M_R) measured in the IP geometry is greater than that in the OOP geometry, which confirms that all the films show a predominant IP magnetization and hence easier to saturate along the plane. The saturation magnetization (M_S) calculated from the initial curves shows increasing trend with the increase in film thickness that is in agreement with the previous results obtained from ferrimagnetic thin films [35,36]. The effective anisotropy constant (K_{eff}) is calculated by subtracting the area under the OOP initial curve from the IP initial curve (see Fig. 1S) [35]. Hence, positive values of K_{eff} quantitatively indicate the presence of weak IP anisotropies in the films. Surprisingly, the evolution of stripe domains and development of weak OOP anisotropy with increasing film thickness were reported previously for Gd-Fe thin films [37]. This is unusual for magnetic films with relatively higher thickness. Such a domain feature was not observed from magnetic force microscopy in the present films with the specified stoichiometry, but the decrease in K_{eff} hints about a change in the orientation of magnetization for the thicker films. The quantitative confirmation about the anisotropy and the direction of magnetization will be discussed further in light of magnetization dynamics.

B. Experimental details for dynamic measurements

We have used a two-color pump-probe technique in the TRMOKE experiment. Here, the fundamental laser beam, generated from a (Tsunami: Spectra Physics, $\lambda = 800$ nm, pulse width ≈ 80 fs, repetition rate $= 80$ MHz, spot size $\approx$ 800 nm) femtosecond laser cavity, is exploited to probe the polar Kerr rotation of the sample and the second harmonic of the fundamental beam ($\lambda = 400$ nm, pulse width $\approx$ 100 fs, repetition rate $= 80$ MHz, spot size $\approx 1\ \mu$m) excites the magnetization dynamics [12]. The time delay between the pump and probe pulse is indicated by Δt. For all experiments, the probe fluence is kept fixed at ≈ 2 mJ/cm^2 and the pump fluence is fixed at ≈ 15 mJ/cm^2. A large static field is applied to saturate the samples along the direction of the field

TABLE I. Stoichiometry, R_q, H_C, M_R, M_S, and K_{eff} for Gd-Fe thin films with different thicknesses are shown.

Film thickness (nm)	Stoichiometry (atomic %)	R_q (nm)	H_C (Oe)		M_R (emu/cm^3)		M_S (emu/cm^3)	K_{eff} (erg/cm^3)
			IP	OOP	IP	OOP		
20	$Gd_{12.7}Fe_{87.3}$	0.7	13	114	53	20	129	1.87×10^5
50	$Gd_{10.2}Fe_{89.8}$	1.0	55	144	48	4	131	1.45×10^5
100	$Gd_{12.1}Fe_{87.9}$	0.8	12	59	59	11	148	0.49×10^5

(>5 kOe) and then its magnitude (H) is varied according to the experimental requirement. During this experiment, the orientation of the $H(\theta_H)$ is varied from OOP to IP [as shown in Fig. 1(b)]. Here, we have considered $\theta_H = 21°$, 50°, and 88° as OOP, tilted, and IP configuration. The probe beam falls collinearly with the pump beam through the same microscope objective (N. A. = 0.65) and measures the magnetization dynamics from a uniformly excited region from the sample. The detection assembly allows the measurement of Kerr rotation and reflectivity simultaneously by avoiding the breakthrough of one signal to another. The time-resolved Kerr rotation data for a 20-nm-thick Gd-Fe thin film is presented in Fig. 1(c). Initially the magnetization of the entire Gd-Fe sublattice system is aligned by the combination of anisotropy field and bias magnetic field and its orientation is indicated by θ_M in Fig. 1(b). The rapid quenching of magnetization just after arrival of the pump pulse is known as the ultrafast demagnetization [7] [regime I, Fig. 1(c)]. The thermalization between electron and lattice results in fast remagnetization within a few picoseconds (regime II). The heat-induced changes in saturation magnetization and anisotropy compel the magnetization to move to a new equilibrium direction. During the cooling process, a laser induced demagnetization field exerts a torque in the magnetization and triggers damped precessional motion of the magnetization towards the previous equilibrium directions [11]. The energy dissipation from lattice to surrounding results in slow remagnetization and introduces a biexponential background with the magnetization precession (regime III). The timescales for ultrafast demagnetization and fast remagnetization for a 20-nm-thick film were obtained as about 300 fs and 1 ps (see Fig. 2S), respectively, from the fitting of experimental data by using a simplified expression

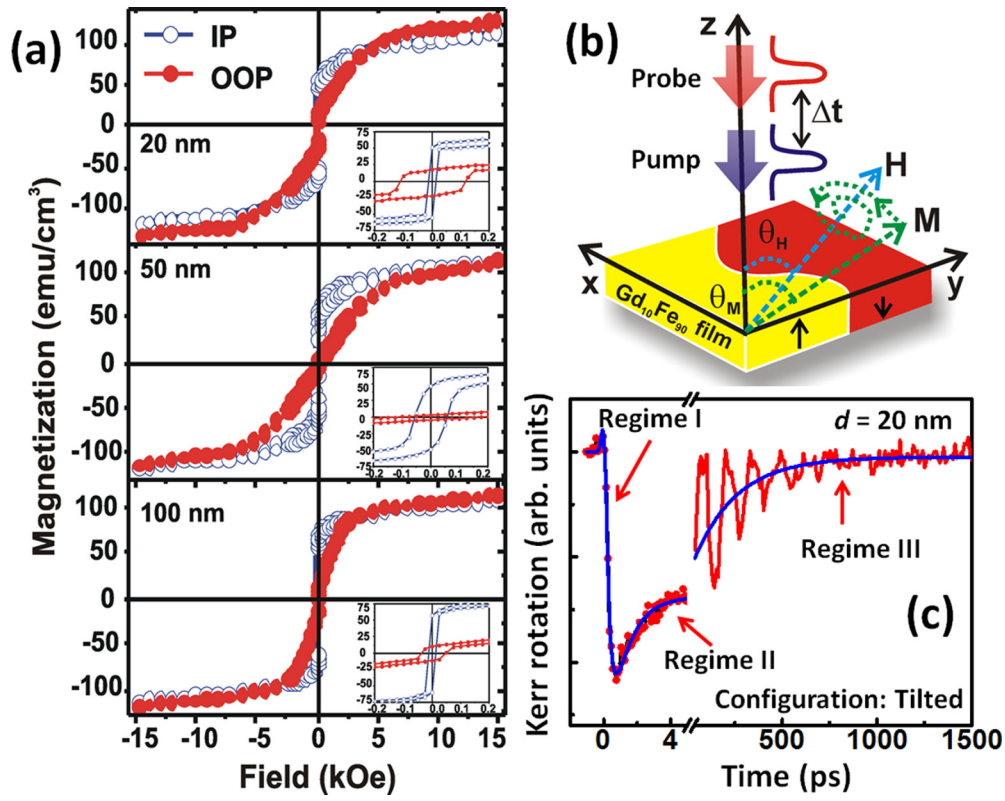

FIG. 1. (a) Hysteresis loops measured by using VSM in OOP and IP configurations for film thickness, $d = 20$, 50, and 100 nm. The nature of magnetization reversal is more prominently shown in the plots provided in the insets. (b) Schematic of experimental geometry used in TRMOKE microscopy. (c) Time-resolved Kerr rotation data showing three different temporal regimes for a 20-nm-thick Gd-Fe film for the tilted configuration of the magnetic field. Blue solid lines represent the fitted curves. Data points in regime I and II are fitted using the three temperature model (Eq. S1) describing ultrafast demagnetization and fast remagnetization, respectively. The exponential fit in regime III corresponds to the slow remagnetization due to energy dissipation from the lattice to the surrounding.

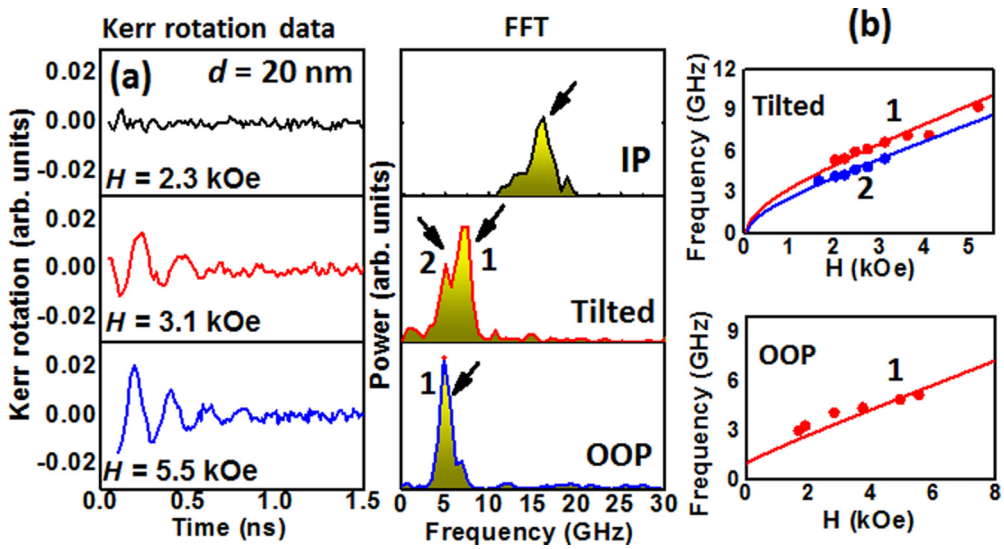

FIG. 2. (a) Background subtracted time-resolved Kerr rotation data and the corresponding FFT spectra for $d = 20$ nm in IP, tilted, and OOP configurations. The magnetic modes are marked with black arrows as well as associated mode numbers. The magnitudes of the bias magnetic fields are indicated in each panel. (b) Bias magnetic field dependence of precessional frequency is presented for tilted and OOP configurations. Solid lines correspond to the Kittel fit.

of the three temperature model [35,38]. Earlier reports show that the TM demagnetizes faster than the RE element and forms a ferromagnetic like state for a short period of time due to the antiferromagnetic interaction between Gd and Fe atoms [22,39], which justifies the demagnetization time obtained in our system. The slow remagnetization time is obtained at about 220 ps. From the background subtracted precessional data we obtain both the precession frequency and decay time of precessional amplitude. The interval between the successive pump pulses is about 12 ns, which ensures the full recovery of the magnetization after it is perturbed. Also, we do not expect any significant reduction of the magnetization of the Gd-Fe thin films for the laser fluence used in the experiment. This is confirmed due to the absence of any significant temporal chirping of the precessional frequency as observed in Ref. [19].

III. RESULTS AND DISCUSSIONS

A. Bias magnetic field dependence of precessional frequency

The magnitude and orientation of the bias magnetic field is varied to obtain field dispersion of the precessional frequency, which is equivalent to ferromagnetic resonance (FMR) in the magnetic system. We performed a fast Fourier transformation (FFT) of the precessional data to obtain the SW spectra in the frequency domain, for $d = 20$ and 100 nm (as shown in Figs. 2 and 3). For the IP configuration the reduction in precessional amplitude leads to a poor signal-to-noise ratio for both samples. As the bias magnetic field is tilted in the OOP direction the precessional amplitude increases and we observed a time-resolved Kerr rotation showing superposition of multiple SW modes. The number of peaks varies for different magnitude and orientations of the bias magnetic field.

For $d = 20$ nm, mostly single mode with reasonable power is observed in the spectra whose frequency decreases with decreasing H for OOP configuration. Another lesser intensity mode with different slope in the field-dispersion curve appears in the low field regime for the tilted configuration (see Fig. 2). At the IP configuration the dominance of nonmagnetic noise has suppressed the features of magnetic peaks. For $d = 100$ nm, there appear three, two, and single modes within our experimental field regime for IP, tilted. and OOP configurations, respectively (Fig. 3). The presence of few spurious peaks in the spectra is found in the IP configuration, which disappears as the field is rotated towards OOP direction. Mode 3 in the IP configuration and mode 2 in the tilted configuration disappear in the low field regime.

To investigate the anisotropic behavior of these modes, we have fitted our experimental data points using the following form of the Kittel formula [40]:

$$f = \frac{\gamma}{2\pi}\sqrt{(H_1 \times H_2)}, \tag{1}$$

$$H_1 = H\mathrm{Cos}(\theta_H - \theta_M) - 4\pi M_{\mathrm{eff}}\mathrm{Cos}^2(\theta_M), \tag{2}$$

$$H_2 = H\mathrm{Cos}(\theta_H - \theta_M) - 4\pi M_{\mathrm{eff}}\mathrm{Cos}(2\theta_M). \tag{3}$$

Here, f is the precessional frequency, $\gamma = g\mu_B/\hbar$ is the gyromagnetic ratio, and g is the Lande g-factor. H, θ_{H}, and θ_{M} are the parameters, already described before. M_{eff} is the effective magnetization, which can be expressed as

$$4\pi M_{\mathrm{eff}} = 4\pi M_s - H_\perp, \tag{4}$$

where $H_\perp = \frac{2K_\perp}{M_s}$ is the OOP anisotropy field and $K_\perp$ is the anisotropy constant. M_{S} is the saturation magnetization of the samples at room temperature obtained from VSM measurement. θ_{M} during onset of dynamics can be found, by solving the following equation numerically:

$$\mathrm{Sin}\,(2\theta_M) = (2H/4\pi M_{\mathrm{eff}})\,\mathrm{Sin}\,(\theta_M - \theta_H), \tag{5}$$

where the IP azimuthal angle for bias magnetic field and magnetization should be same with respect to the IP coordinates.

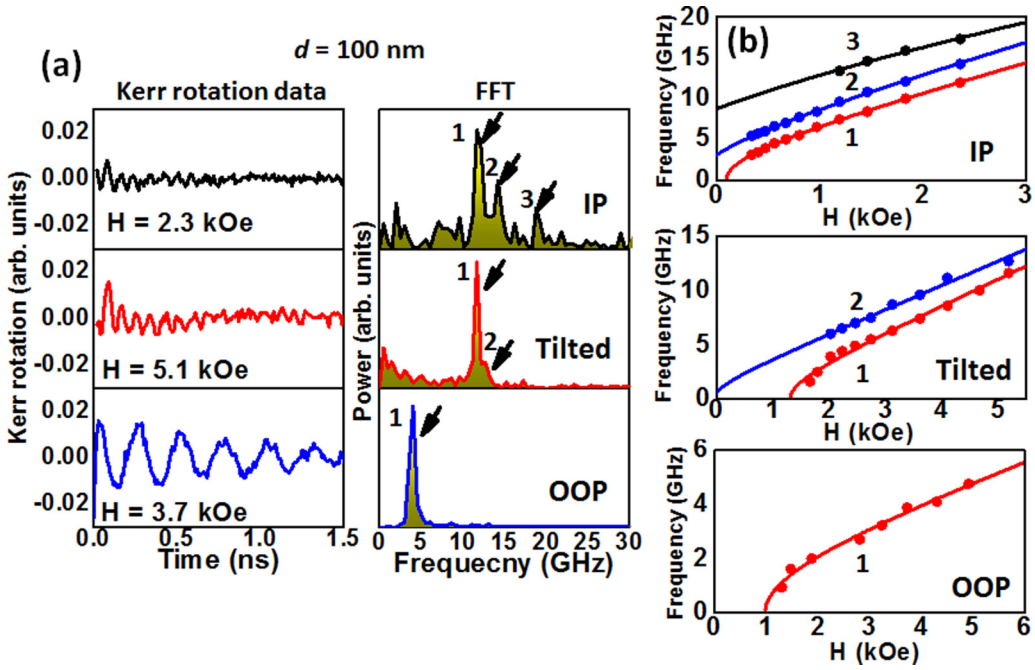

FIG. 3. (a) Background subtracted time-resolved Kerr rotation data and corresponding FFT spectra for $d = 100$ nm in the IP, tilted, and OOP configurations. The magnetic modes are marked with black arrows as well as associated mode numbers. The magnitudes of bias magnetic field are indicated in each panel. (b) Bias magnetic field dependence of the precessional frequency is presented. Solid lines correspond to the Kittel fit.

Combining the abovementioned equations, we have fitted the Kittel mode for different field orientations of both the samples and the fitting parameters have been recorded in Table II.

The M_S values obtained from fitting differ with the saturation magnetization within $\pm 10\%$. The magnetization follows mostly the orientation of bias magnetic field, though the combined effect of anisotropy and external field controls the tilt of magnetization. The positive sign of the anisotropy constant demonstrates an evolution of OOP anisotropy, although its magnitude is comparatively lower than the conventional PMA systems, such as, Co/Pd multilayers, etc. [41]. Although the sources of OOP anisotropy in amorphous RE-TM films are a topic of debate, previous studies explained the development of PMA in thicker Gd-Fe films with the presence of labyrinth-like magnetic domains, the width of which increases with the increase in film thickness along with the simultaneous reduction in domain wall width. The energetics, derived from micromagnetic simulations elucidated the dominant role of dipolar coupling behind the development of this anisotropy in thicker films [37].

We fitted the higher frequency modes appeared for 100-nm-thick film using the following formula of PSSW modes [42,43]:

$$f = \frac{\gamma}{2\pi}\sqrt{\left(H\mathrm{Cos}(\theta_H-\theta_M) - 4\pi M_{\mathrm{eff}}\mathrm{Cos}^2(\theta_M) + \frac{2A}{M_s}\left(\frac{n\pi}{d}\right)^2\right)\left(H\mathrm{Cos}(\theta_H-\theta_M) - 4\pi M_{\mathrm{eff}}\mathrm{Cos}(2\theta_M) + \frac{2A}{M_s}\left(\frac{n\pi}{d}\right)^2\right)}. \quad (6)$$

Here, A, n, and d, are the exchange stiffness constant, order of PSSW mode, and thickness of the film, respectively. The other parameters have their usual meaning. This formula holds for the experimental configuration with $\theta_H \approx \theta_M \approx 90^\circ$. From the fit we have confirmed that mode 2 for the IP and tilted configurations is the first order PSSW mode ($n = 1$) for this thick film. Mode 3 for the IP configuration is the second order PSSW with $n = 2$. The exchange stiffness constant is found to be $A = 2.6 \times 10^{-7}$ erg/cm, which agrees well with the reported values for Gd-Fe thin films [32]. It is worth mentioning here that we also observed a lower frequency mode in the close vicinity of the Kittel mode in the 20-nm-thick film. This mode is of magnetic origin as confirmed from its field dispersion. However, the field dispersion of these modes could not be fitted well with reasonable parameters. It may arise from the magnetic inhomogeneity developed in the system. A slight change in anisotropy sometimes along the thickness of the film cannot be ruled out. The Kittel fit of this mode with $M_S = 111$ emu/cm^3 and $K_\perp = 0.8 \times 10^5$ erg/cm^3, justifies the above speculation. There is the possibility of inhomogeneous growth of the films with nonuniformity in the elemental composition along the thickness [34], which can cause the appearance of modes other than the Kittel mode. Moreover, the strength of the dipolar field is more at the surface of the film due to the closure of magnetic lines of the force through the top and the bottom of the sample. This may

TABLE II. Parameters corresponding to field dispersion of uniform Kittel modes in the frequency spectra of Gd-Fe samples having thickness 20 and 100 nm, are presented.

Film thickness (nm)	Parameters obtained from fitting				
	θ_H (°)	θ_M (°)	g	M_S (emu/cm^3)	$K_\perp$ (erg/cm^3)
20	21	73	2.0	127	0.9×10^5
	50	73	2.0	137	0.9×10^5
100	21	67	2.0	152	1.6×10^5
	50	70	2.0	152	1.6×10^5
	88	86	2.0	160	1.3×10^5

result in nonuniformity in magnetization along the thickness, where the net magnetization at the surface is less compared to the middle layers and hence may display weaker domain contrast.

The bias-field dependent precessional magnetization dynamics for a 50-nm-thick film in the tilted and OOP configurations are presented in the Supplemental Material (see Fig. 3S) [35]. In the IP configuration the signal-to-noise ratio is poor in the time-resolved data. The precessional data is noisy and damps very quickly after a few tens of picoseconds, making a precise determination of the precessional frequency from the FFT spectra very difficult. In the tilted configuration, we are able to identify splitting of a peak where the higher frequency mode may have a PSSW nature. In the OOP configuration, the picosecond precession shows a single frequency oscillation [Fig. 3S(a)] [35]. The precessional frequencies are plotted as a function of bias magnetic field magnitude. Figure 3S(b) shows that for tilted and OOP configurations, the experimental data points are fitted well with the Kittel formula, the extracted values of M_S are about 130 emu/cm^3, and $K_\perp$ is about 1.15×10^5 erg/cm^3, which indicates systematic development of the OOP anisotropy. All the modes cannot be fitted with the Kittel formula. The damping of the Kittel mode in the OOP configuration has shown an increasing trend with decrease in frequency [Fig. 3S(c)] [35].

B. Analyses of damping

In order to extract the decay time and Gilbert damping of the precessional oscillations quantitatively, the sum of multiple damped sinusoidal functions is applied [44] and the time variation of Kerr rotation angle ($\Delta\theta_K$) can be expressed as

$$\Delta\theta_K \propto \sum_{i=1}^{m} A_i\, e^{(-\frac{t}{\tau_i})} \mathrm{Sin}(2\pi f_i t + \phi_i), \tag{7}$$

where A_i, τ_i, f_i, ϕ_i are the precessional amplitude, decay time, frequency, and initial phase of oscillation of the i^{th} mode, and m is the mode number. This is used to fit the transient magnetization curves if there is the clear existence of more than one SW mode ($1 \leqslant m \leqslant 3$). In other cases, a single damped sinusoidal function is applied to give a good fit to the curves. For example, in the 20-nm-thick film, the intensity of a low frequency mode (mode 2) observed for the tilted configuration may not have any significant contribution to the dephasing of the precessional amplitude of the Kittel mode (mode 1). Thus for, both the OOP and tilted configurations

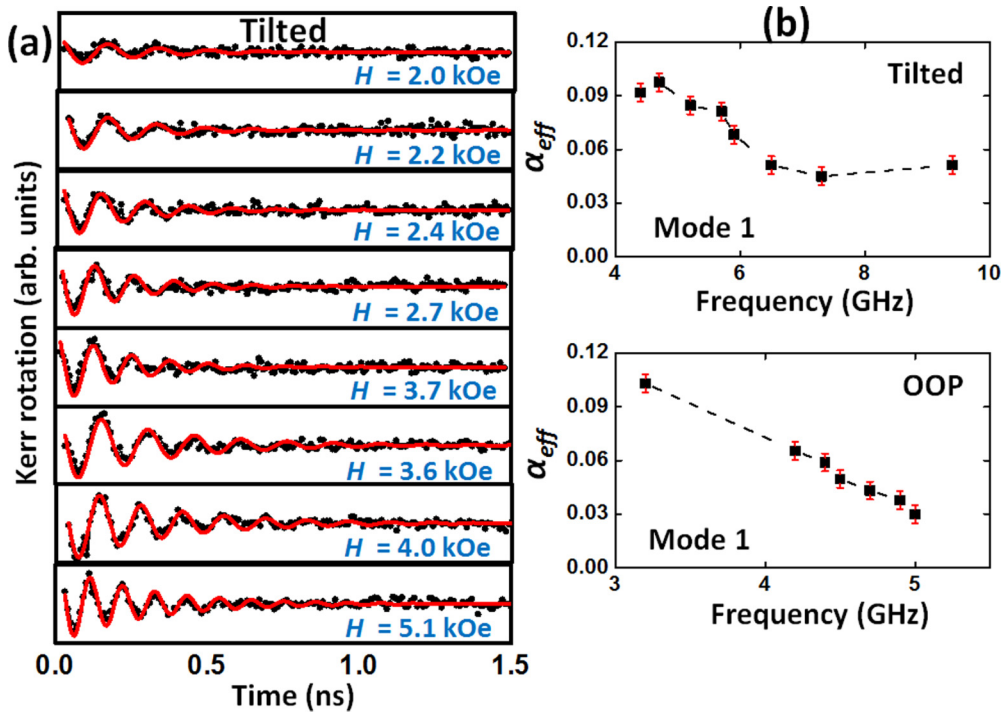

FIG. 4. (a) Background subtracted time-resolved Kerr rotation data and the corresponding fit with a damped sine function for $d = 20$ nm in the tilted configuration. (b) The variation of effective damping with precessional frequency in the tilted and OOP configurations. The solid lines are fits. Dotted lines are guides to the eye.

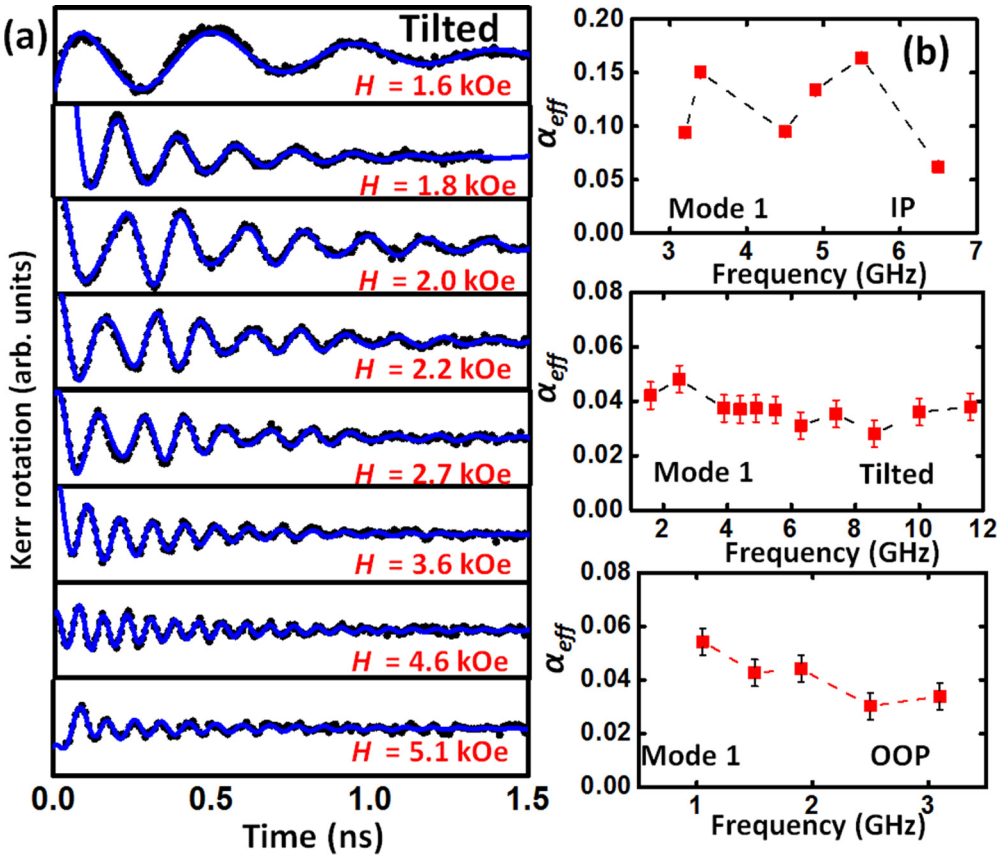

FIG. 5. (a) Background subtracted time-resolved Kerr rotation data and corresponding fit with a damped sine function for $d = 100$ nm in the tilted configuration. (b) The variation of effective damping with precessional frequency in the IP, tilted, and OOP configurations. The solid lines are fits. Dotted lines are guides to the eye. Some of the error bars may not be visible as those are merged within the size of points indicated in the plot.

time-resolved data are fitted with single damped sinusoidal function [Fig. 4(a)]. We have plotted the variation of decay time (τ) with precessional frequency in order to understand the bias magnetic field dependence of damping for this system in Fig. 6. In the tilted and OOP configurations, the decay time is found to be almost constant at around 0.3 ns. We have extracted the damping of these modes from the following expression [43]:

$$\alpha_{\text{eff}} = \frac{1}{\tau\gamma(H - \frac{k_\perp}{\mu_0 M_s} + 4\pi M_s/2)}. \tag{8}$$

Here, α_{eff} is the effective damping of the system, which consists of intrinsic and extrinsic contributions. Other parameters have their usual meaning. In Fig. 4(b), the variation of damping with precessional frequency is plotted corresponding to each field orientation. For the tilted and OOP configurations, effective damping increases rapidly with decreasing frequency and the enhancement is almost three times their intrinsic values. Here, we believe that for $f > 5$ GHz, the bias magnetic field is high enough to suppress any additional effects present in the sample that can extrinsically modulate the damping [44]. Thus for the tilted configuration, damping shows a constant value for $f > 5$ GHz. As the saturation magnetization for this sample is quite less ($\sim$130 emu/cm^3), the field values of about 4 kOe can be considered to be sufficiently high.

For 100-nm-thick Gd-Fe film, time-resolved data are fitted with a damped sinusoidal function consisting of multiple frequencies [see Fig. 5(a)] and Eq. (7) has been exploited to fit the precessional oscillations. The decay times for the Kittel as well as PSSW modes for IP configuration are on the order of 0.4 to 0.8 ns. The extracted damping values are significantly high (α_{eff} increased up to 0.2) [as shown in Fig. 5(b)]. However for the tilted and OOP configurations, the decay time of the Kittel mode has been increased from 0.5 ns to almost 1.0 ns within the experimental frequency range. For the first order PSSW mode in the tilted configuration, the trend is the opposite (shown in Fig. 5) where decay time decreased with the decrease in frequency. For the IP configuration, we would like to mention that the decay times extracted from the three-frequency fitting (at higher field) may contain relatively large error due to nontrivial fitting conditions adopted with multiple fitting parameters and the smaller precessional amplitude of the higher frequency modes. Effective damping extracted for the Kittel mode shows increasing nature with decreasing frequency and attains a constant value at the higher field regime.

The Gilbert damping parameter is mainly responsible for bringing the system into an equilibrium state. The effective damping parameter depends on several extrinsic factors,

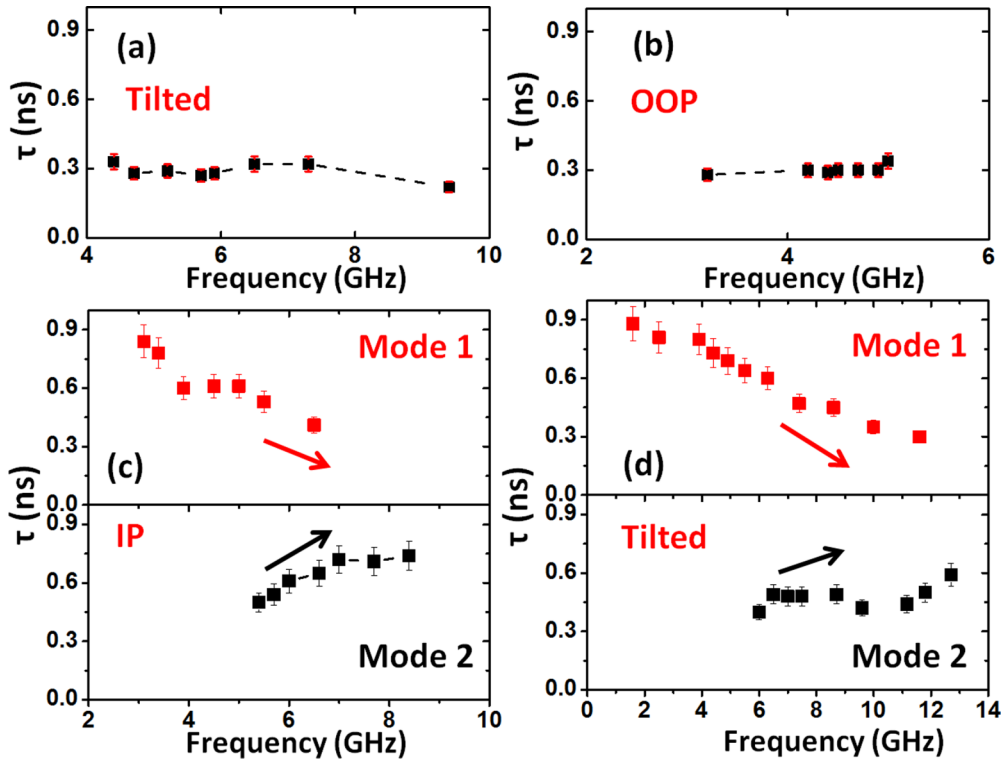

FIG. 6. The variation of decay time (τ) with the precessional frequency of mode 1 (Kittel mode) for the Gd-Fe film with thickness, $d = 20$ nm in (a) the tilted and (b) the OOP configurations. Variation of τ for mode 1 and mode 2 for the Gd-Fe film with thickness, $d = 100$ nm in (c) the IP and (d) the tilted configurations is shown. The arrow indicates an opposite trend in the variation of τ. The dotted lines are guides to the eye.

including composition of the RE and TM in the sample. Due to the presence of half-filled $4f$ shell in Gd, the direct spin-lattice excitation is absent and the damping occurs only through the interaction with the conduction band electrons. Hence, the damping of the Gd sublattice is found to be very low. Natural damping of the Fe sublattice lies in the vicinity of $\alpha_{\mathrm{Fe}} = 0.02$. In our experiments, the extracted effective damping parameters lie in the range of 0.02 to 0.15 ($0.02 \leqslant \alpha_{\mathrm{eff}} \leqslant 0.15$) within our experimental field regime [8,31]. As the samples are Fe rich, the higher values of damping of the Kittel mode in some field orientation indicate the presence of an extrinsic contribution other than the intrinsic Gilbert damping in these films. We discuss the possibilities below.

In the low frequency regime the damping is similar for both the films and is on the order of 0.15. As the films show roughness below 1 nm (Table I) with no identifiable feature or ripple in the surface, the contribution of roughness to the higher damping values can probably be ruled out. Sometimes the TM film with RE doping can contain specific regions with nonuniform RE concentration. Magnetic inhomogeneity can sometimes cause two-magnon scattering (TMS) where the resonant FMR mode (usually $k \sim 0$) scatters into other magnons having the same frequency. In the presence of magnetic defects, magnon momentum is not generally conserved, and the relaxation parameter becomes strongly frequency dependent. Thus, the TMS causes enhancement of damping in the lower frequency regime [44,14]. Specifically, TMS is a bulk effect and its magnitude depends on the angle of the magnetization with respect to the IP crystallographic axis (if any). In our experiments, we have found an increase in the effective damping with the decrease in frequency with its slope varying for different bias magnetic field orientation (Figs. 4 and 5). This qualitatively indicates that extrinsic contributions, including TMS, can be present in the damping values. The damping of the Kittel mode for the Gd-Fe thin films is reported to be less compared to the high values observed in our samples [23]. However, the presence of additional higher frequency PSSW modes may open up additional energy dissipation channels, effectively increasing the damping values in our study. Figure 6 shows that the decay time of the Kittel mode for the 20-nm-thick Gd-Fe film is nearly invariant with the precessional frequency [44]. However, the situation changes for the IP and tilted configurations for the 100-nm-thick film, where a decrease in τ of the Kittel mode (mode 1) simultaneously takes place with the increase in τ of the PSSW mode (mode 2), with an increase in frequency, indicating a strong correlation between the two. This phenomenon hints that the possibility for energy transfer from the uniform Kittel mode to the PSSW mode exists [15]. The absence of PSSW modes in the lower frequency regime is probably due to the presence of TMS, caused by the magnetic inhomogeneities in the film [34,45]. However, we have not been able to isolate various contributions, including TMS, to the observed damping in our study. The significant tunability of damping by bias magnetic field for the Gd-Fe system can be important for various possible applications. A higher value of damping can suppress the unwanted ringing after a

precessional switching. On the other hand, lower damping is advantageous for long distance SW propagation and smaller write-current in spin-transfer torque based magnetic random-access memory (STT-MRAM) devices.

IV. CONCLUSIONS

A systematic investigation of ultrafast magnetization dynamics has been presented for Gd-Fe thin films of different thicknesses. The demagnetization time was found to be about 300 fs for these thin films. A special emphasis has been provided to the study of precessional magnetization dynamics as a function of magnitude and orientation of the bias magnetic field. Our time-resolved results show a development of weak OOP anisotropy with increasing film thickness, which is complemented by static magnetization measurements. A large tunability of effective damping of the system has been obtained with the variation in bias magnetic field, which could be due to extrinsic effects such as, TMS, magnetic inhomogeneity, impurity scattering, and multimodal dephasing. The presence of higher order PSSW modes along with the uniform Kittel mode was evidenced for the 100-nm-thick film. Intermode energy transfer between PSSW modes and the uniform Kittel mode is found to be a possible mechanism behind the modification of decay times for the thicker film. The extensive study of magnetization dynamics presented here may lead to the development of magnonic and spintronic devices based on RE-TM thin films.

ACKNOWLEDGEMENTS

We gratefully acknowledge the financial support from S. N. Bose National Centre for Basic Sciences (Grants No. SNB/AB/18-19/211). S.M. acknowledges DST for the INSPIRE fellowship (Award No. IF140998). J.R.M. acknowledges the financial support from SERB, Government of India, through Grant No. EMR/2016/006794.

[1] J. A. Katine, F. J. Albert, R. A. Buhrman, E. B. Myers, and D. C. Ralph, Phys. Rev. Lett. **84**, 3149 (2000).
[2] H. Ohno, D. Chiba, F. Matsukura, T. Omiya, E. Abe, T. Dieti, Y. Ohno, and K. Ohtani, Nature (London) **408**, 944 (2000).
[3] C. D. Stanciu, F. Hansteen, A.V. Kimel, A. Kirilyuk, A. Tsukamoto, A. Itoh, and Th. Rasing, Phys. Rev. Lett. **99**, 047601 (2007).
[4] T. Gerrits, H. A. M. van den Berg, J. Hohlfeld, L. Bär, and Th. Rasing, Nature (London) **418**, 509 (2002).
[5] S. Kaka and S. E. Russek, Appl. Phys. Lett. **80**, 2958 (2002).
[6] H.W. Schumacher, C. Chappert, P. Crozat, R. C. Sousa, P. P. Freitas, J. Miltat, J. Fassbender, and B. Hillerbrands, Phys. Rev. Lett. **90**, 017201 (2003).
[7] E. Beaurepaire, J.-C. Merle, A. Daunois, and J.-Y. Bigot, Phys. Rev. Lett. **76**, 4250 (1996).
[8] C. D. Stanciu, A. V. Kimel, F. Hansteen, A. Tsukamoto, A. Itoh, A. Kirillyuk, and Th. Rasing, Phys. Rev. B **73**, 220402(R) (2006).
[9] C.-H. Lambert, S. Mangin, B. S. Varaprasad, Y. K. Takahashi, M. Hehn, M. Cinchetti, G. Malinowski, K. Hono, Y. Fainman, M. Aeschilmann, and E. E. Fullerton, Science **345**, 1337 (2014).
[10] S. Mangin, M. Gottwald, C.-H. Lambert, D. Steli, V. Uhlíř, L. Pang, M. Hehn, S. Alebrand, M. Cinchetti, G. Malinowski, Y. Fainman, M. Aeschilmann, and E. E. Fullerton, Nat. Mater. **13**, 286 (2014).
[11] M. van Kampen, C. Jozsa, J. T. Kohlhepp, P. LeClair, L. Lagae, W. J. M. de Jonge, and B. Koopmans, Phys. Rev. Lett. **88**, 227201 (2002).
[12] A. Barman and J. Sinha, *Spin Dynamics and Damping in Ferromagnetic Thin Films and Nanostructures* (Springer, Switzerland, 2018).
[13] A. Barman and A. Haldar, *Time-Domain study of Magnetization Dynamics in Magnetic Thin Films and Micro- and Nanostructures*, Solid State Phys, Vol. 65 (Elsevier, Burlington, 2014), pp. 1–108.
[14] G. Woltersdorf, M. Buess, B. Heinrich, and C. H. Back, Phys. Rev. Lett. **95**, 037401 (2005).
[15] S. N. Panda, S. Mondal, J. Sinha, S. Choudhury, and A. Barman, Sci. Adv. **5**, eaav7200 (2019).
[16] Y. Zhao, Q. Song, S. H. Yang, T. Su, W. Yuan, S. S. P. Parkin, J. Shi, and W. Han, Sci. Rep. **6**, 22890 (2016).
[17] S. Mondal, S. Choudhury, N. Jha, A. Ganguly, J. Sinha, and A. Barman, Phys. Rev. B **96**, 054414 (2017).
[18] G. M. Muller, M. Munzenberg, G.-X. Miao, and A. Gupta, Phys. Rev. B **77**, 020412(R) (2008).
[19] S. Mondal and A. Barman, Phys. Rev. Appl. **10**, 054037 (2018).
[20] A. Kirilyuk, A. V. Kimel, and Th. Rasing, Rep. Prog. Phys. **76**, 026501 (2013).
[21] A. R. Khorsand, M. Savoini, A. Kirilyuk, A. V. Kimel, A. Tsukamoto, A. Itoh, and Th. Rasing, Phys. Rev. Lett. **110**, 107205 (2013).
[22] I. Radu, K. Vahaplar, C. Stamm, T. Kachel, N. Pontius, H. A. Durr, T. A. Ostler, J. Barker, R. F. L. Evans, R. W. Chantrell, A. Tsukamoto, A. Itoh, A. Kirilyuk, Th. Rasing, and A. V. Kimel, Nature (London) **472**, 205 (2011).
[23] J. Sizeland, Ph.D. thesis, Crystallographic and magneto-dynamic characterization of thin film spintronic materials, University of York Press, UK, 2015.
[24] J. Miguel, Ph.D. thesis, Static and dynamic x-ray resonant magnetic scattering studies on magnetic domains, University of Amsterdam Press, The Netherlands, 2015.
[25] J. C. Suits, R. D. Rugar, and C. J. Lin, J. Appl. Phys. **64**, 252 (1988).
[26] W. H. Meiklejohn, Proc. IEEE **74**, 1570 (1986).
[27] A. K. Biswas, H. Ahmad, J. Atulasimha, and S. Bandyopadhyay, Nano Lett. **17**, 3478 (2017).
[28] S. Mondal, M. A. Abeed, K. Dutta, A. De, S. Sahoo, A. Barman, and S. Bandyopadhyay, ACS Appl. Mater. Interfaces **10**, 43970 (2018).

[29] J. Becker, A. Tsukamoto, A. Kirilyuk, J. C. Maan, Th. Rasing, P. C. M. Christianen, and A. V. Kimel, Phys. Rev. B **92**, 180407(R) (2015).

[30] R. Salikhov, A. Alekhin, T. Parpiiev, T. Pezeril, D. Makarov, R. Abrudan, R. Meckenstock, F. Radu, M. Farle, H. Zabel, and V. V. Temnov, Phys. Rev. B **99**, 104412 (2019).

[31] K. Nishibayashi, K. Kuga, and H. Munekata, AIP Adv. **3**, 032107 (2013).

[32] J. Miguel, J. F. Peters, O. M. Toulemonde, S. S. Dhesi, N. B. Brookes, and J. B. Goedkoop, Phys. Rev. B **74**, 094437 (2006).

[33] A. Talapatra, J. Arout Chelvane, and J. Mohanty, J. Magn. Magn. Mater. **448**, 360 (2018).

[34] A. Talapatra, J. Arout Chelvane, B. Satpati, S. Kumar, and J. Mohanty, J. Alloy. Compd. **774**, 1059 (2019).

[35] See Supplemental Material at http://link.aps.org/supplemental/10.1103/PhysRevB.100.054436 for showing the partial *M*-H curves for the Gd-Fe films, modeling of ultrafast demagnetization for a 20-nm-thick Gd-Fe film, and bias magnetic field dependent magnetization dynamics for a 50-nm-thick Gd-Fe film.

[36] B. Hebler, A. Hassdenteufel, P. Reinhardt, H. Karl, and M. Albrecht, Front. Mater. **3**, 8 (2016).

[37] A. Talapatra, J. Arout Chelvane, and J. Mohanty, J. Magn. Magn. Mater. **489**, 165469 (2019).

[38] F. Dalla Longa, J. T. Kohlhepp, W. J. M. de Jonge, and B. Koopmans, Phys. Rev. B **75**, 224431 (2007).

[39] I. Radu, C. Stamm, A. Eschenlohr, F. Radu, R. Abrudan, K. Vahaplar, T. Kachel, N. Pontius, R. Mitzner, K. Holldack, A. Föhlisch, T. A. Ostler, J. H. Mentink, R. F. L. Evans, R. W. Chantrell, A. Tsukamoto, A. Itoh, A. Kirilyuk, A. V. Kimel, and Th. Rasing, Spin **5**, 1550004 (2015).

[40] S. Mizukami, H. Abe, D. Watanabe, M. Oogane, Y. Ando, and T. Miyazaki, Appl. Phys. Exp. **1**, 121301 (2008).

[41] S. Pal, B. Rana, O. Hellwig, T. Thompson, and A. Barman, Appl. Phys. Lett. **98**, 082501 (2011).

[42] B. Samantaray, A. K. Singh, C. Banerjee, A. Barman, A. Perumal, and P. Mandal, IEEE. Trans. Magn. **52**, 2003104 (2016).

[43] J. Walowski, M. D. Kaufmann, B. Lenk, C. Hamann, J. McCord, and M. Münzenberg, J. Phys. D **41**, 164016 (2008).

[44] Z. Chen, Y. Yan, S. Li, X. Xu, Y. Jiang, and T. Lai, Sci. Rep. **7**, 42513 (2017).

[45] X. Lu, L. J. Atkinson, B. Kuerbanjiang, B. Liu, G. Li, Y. Wang, J. Wang, X. Ruan, J. Wu, R. F. L. Evans, V. K. Lazarov, R. W. Chantrell, and Y. Xu, Appl. Phys. Lett. **114**, 192406 (2019).